Follow us @BoneJointRes

Freely available online OPEN ACCESS

BJR

BONE FRACTURE

PHOSPHO1 is essential for normal bone fracture healing

AN ANIMAL STUDY

M. W. Morcos,
H. Al-Jallad,
J. Li,
C. Farquharson,
J. L. Millán,
R. C. Hamdy,
M. Murshed

McGill University, Montreal, Quebec, Canada

Objectives

Bone fracture healing is regulated by a series of complex physicochemical and biochemical processes. One of these processes is bone mineralization, which is vital for normal bone development. Phosphatase, orphan 1 (PHOSPHO1), a skeletal tissue-specific phosphatase, has been shown to be involved in the mineralization of the extracellular matrix and to maintain the structural integrity of bone. In this study, we examined how PHOSPHO1 deficiency might affect the healing and quality of fracture callus in mice.

Methods

Tibial fractures were created and then stabilized in control wild-type (WT) and *Phospho1*$^{-/-}$ mice (n = 16 for each group; mixed gender, each group carrying equal number of male and female mice) at eight weeks of age. Fractures were allowed to heal for four weeks and then the mice were euthanized and their tibias analyzed using radiographs, micro-CT (μCT), histology, histomorphometry and three-point bending tests.

Results

The μCT and radiographic analyses revealed a mild reduction of bone volume in *Phospho1*$^{-/-}$ callus, although it was not statistically significant. An increase in trabecular number and a decrease in trabecular thickness and separation were observed in *Phospho1*$^{-/-}$ callus in comparison with the WT callus. Histomorphometric analyses showed that there was a marked increase of osteoid volume over bone volume in the *Phospho1*$^{-/-}$ callus. The three-point bending test showed that *Phospho1*$^{-/-}$ fractured bone had more of an elastic characteristic than the WT bone.

Conclusion

Our work suggests that PHOSPHO1 plays an integral role during bone fracture repair and may be a therapeutic target to improve the fracture healing process.

Cite this article: *Bone Joint Res* 2018;7:397–405.

Keywords: Bone mineralization, PHOSPHO1, Bone fracture repair, Endochondral ossification, Phospho1-/- mice

Article focus

- The current article uses a genetically modified mouse model (Phospho1-/-) to study the effects of poor bone mineralization on bone fracture healing.

Key messages

- The amount of unmineralized bone is markedly higher at fracture sites in Phospho1-/- mice than that of wild type mice.

Strengths and limitations

- The use of PHOSPHO1 as a pro-mineralization agent may facilitate faster mineralization and healing of fractures.

Introduction

Fractures are common and fracture healing is a complex process, regulated by genetic, biological and mechanical factors, which takes place over a period of weeks to years. Fracture healing may occur through intramembranous ossification, but more commonly, through endochondral ossification, which is typically seen in long bone fractures.[1-4]

Bone forming osteoblasts play a key role in the fracture healing process by regulating the mineralization of the bone extracellular matrix (ECM). A poorly mineralized ECM may lead to improper resorption of the

M. W. Morcos, MD, MSc, Orthopaedic Surgeon,
R. C. Hamdy, MD, MSc, FRCSC, Orthopaedic Surgeon, Division of Paediatric Orthopaedic Surgery, and Department of Medicine, Shriners Hospital for Children and McGill University, Montreal, Quebec, Canada.
H. Al-Jallad, PhD, Research Associate, Division of Paediatric Orthopaedic Surgery, Shriners Hospital for Children, Montreal, Quebec, Canada.
J. Li, PhD, Research Associate, Department of Medicine, McGill University, Montreal, Quebec, Canada.
C. Farquharson, PhD, Professor, Personal Chair of Skeletal Biology, The Roslin Institute, University of Edinburgh, Midlothian, UK.
J. L. Millán, PhD, Professor, Human Genetics Program, Sanford Burnham Prebys Medical Discovery Institute, La Jolla, California, USA.
M. Murshed, PhD, Associate Professor, Department of Medicine, and Faculty of Dentistry, Shriners Hospital for Children and McGill University, Montreal, Quebec H4A 0A9, Canada.

Correspondence should be sent to M. Murshed;
email: monzur.murshed@mcgill.ca

doi: 10.1302/2046-3758.76.BJR-2017-0140.R2

Bone Joint Res 2018;7:397–405.

mineralized callus and eventually to weaker bone with compromised mechanical properties.

Bone mineralization is regulated by both humoral and cellular factors that are produced locally in the tissue. Humoral factors include inorganic phosphate (P_i) and calcium ions, as well as the hormones that regulate their homeostasis.[5,6] The deposition of hydroxyapatite (HA) crystals ($Ca_{10}(PO)_4(OH)_2$) in bone significantly contributes to its unique mechanical and biophysical properties.[7] Osteoblasts regulate ECM mineralization by synthesizing the mineral-scaffolding matrix and producing enzymes that control the nucleation and propagation of mineral crystals.[8]

An essential component in the regulation of bone ECM mineralization is alkaline phosphatase and in particular, tissue non-specific alkaline phosphatase (TNAP/ALPL), which is encoded by the *ALPL* gene.[9] TNAP is a membrane-bound glycoprotein that is present on the surface of mineralizing cells such as osteoblasts.[10] It plays an important role in maintaining the extracellular concentration of inorganic pyrophosphatase (PP_i), a potent inhibitor of ECM mineralization. TNAP splits PP_i into P_i, an essential component of HA, which in turn facilitates the formation and propagation of HA crystals.[11,12] Mutations in *ALPL* can lead to severe impairment of bone and teeth mineralization in humans and in experimental models.[12,13] We have recently shown that during embryonic development, ALPL and a cytosolic phosphatase, Phosphatase, orphan 1 (PHOSPHO1), work cooperatively to facilitate skeletal tissue mineralization.[10,14,15]

PHOSPHO1 is a member of the haloacid dehalogenase (HAD) superfamily of magnesium (Mg^{2+})-dependent hydrolases. It splits phosphoethanolamine (PE) and phosphocholine to produce ethanolamine or choline and P_i.[16,17] The expression of PHOSPHO1 is at least 100-fold higher in mineralized tissues and has been detected in multiple species including in humans and mice.[18-20] Several studies have examined the phenotype of PHOSPHO1-deficient (*Phospho1*$^{-/-}$) mice and found that these mice show abnormal endochondral growth plates and skeletal anomalies including osteomalacia, scoliosis, long bone deformity and spontaneous fractures.[15,21,22] These findings suggest that PHOSPHO1 is an essential regulator of skeletal tissue development and maintenance.

The role of PHOSPHO1 in bone fracture healing and the mechanical properties of the newly formed bone have not been reported previously. Based on our knowledge of the essential role of PHOSPHO1 in bone mineralization, we hypothesize that it plays a critical role in fracture healing. Our results presented here show that PHOSPHO1 activity is necessary during the repair of fractured bones.

Materials and Methods

Mice. Generation of *Phospho1*$^{-/-}$ mice has been described previously.[21] Eight-week-old *Phospho1*$^{-/-}$ mice and wild-type (WT) control mice were used for this study. All mice were generated and maintained at the Shriners animal facility following a protocol approved by the Animal Care and Use Committee of McGill University.

Surgical method. All mice underwent intramedullary nailing of the right tibia at eight weeks of age. A total of 32 mice (16 WT and 16 mutant mice, mixed gender, each group carrying equal number of male and female mice) were used. The surgical procedure was performed under aseptic conditions in the procedure room of the animal facility. The mice were anaesthetized with an isoflurane-oxygen gas mix and kept under anaesthesia throughout the length of the procedure. A 3-mm vertical skin incision was made at the knee and the patellar ligament was exposed. The joint line was identified, and a 26 G needle was inserted into the proximal tibial canal. The internal wire guide of a 25 G spinal needle was then passed through the 26 G needle and down the tibial canal. The 26 G needle was removed leaving the wire within the tibia and the wire was then cut short at the level of the tibial plateau. Through the same skin incision, a mid-shaft tibial osteotomy was produced with extra fine Bonn scissors (Fine Science Tools, Foster City, California). The soft tissues were closed with a single 6-0 vicryl suture and the animals were returned to their cage to recover. Post-operative care included a subcutaneous injection of carprofen (5 μl/g) and 20 μl/g of normal saline. The mouse cage was placed on a heated pad and the mice were allowed to ambulate freely. The animals were closely monitored and any mice showing signs of severe pain, bleeding or swelling were humanely killed.

Sample collection. The analysis of the fractured bones was performed four weeks after surgery. The mice were euthanized, fractured legs were dissected out and the intramedullary nail from the tibia was carefully removed with a needle holder. Tibias destined for micro-CT (μCT) and histological analysis were fixed in buffered formalin overnight and then transferred to 70% ethanol, whilst the tibias destined for mechanical testing were wrapped in paper and stored in phosphate-buffered saline at 4°C until biomechanical testing. Sample distribution for various analyses was as follows: μCT, n = 8 mice/group; radiographs, n = 3 mice/group; histology and histomorphometry, n = 8 mice/group; and three-point bending test, n = 8 mice/group.

Radiographs. Imaging of the tibias was performed using the XPERT radiograph imaging system (Kubtec Medical Imaging, Stratford, Connecticut). The radiograph source was operated at 21 kV and at 550 μA. Samples were scanned at a magnification of ×4.

μCT. Tibia samples in 70% ethanol were subjected to μCT analysis (SkyScan 1172 radiograph micro-tomograph; Skyscan, Kontich, Belgium). All scans were undertaken with the SkyScan 1.5 software at a source voltage of 65 kV and a source current of 153 μA. A

medium camera setting with an aluminium filter was used. The samples were scanned at an image voxel size of 5 μm with a mean scanning time of 30 minutes for each sample. For every 0.45° of sample rotation, three image frames were retained. A total vertical segment of 8 mm was scanned for every sample and generated around 800 consecutive transverse image slices. The generated images were reconstructed using cone-beam reconstruction software (SkyScan) with a beam-hardening correction of 50% and a ring artefact correction of 5%. The reconstructed images were then analyzed using SkyScan 1.11 software.

Histology and histomorphometry. For plastic sectioning, tibia samples were fixed overnight in 10% buffered formalin, pH 7.4, embedded in methyl methacrylate, and sectioned (7 μm thickness). Sections were deplasticized in 2-methoxyethyl acetate and rehydrated in a descending series of alcohols. The sections were stained with von Kossa, followed by van Gieson, staining to detect the mineralized and unmineralized ECM, respectively. Briefly, the slides were first immersed in 1% silver nitrate for five minutes, washed in deionized water, immersed in 5% sodium carbonate in 10% formaldehyde for five minutes, washed in running tap water and finally placed in 5% sodium thiosulfate for five minutes and again washed in running tap water. Next, the slides were stained in van Gieson solution (0.25% fuchsin in 10% glycerol, 0.35% nitric acid and 90% picric acid) for two minutes and dehydrated in an ascending series of alcohols and mounted using a xylene-based mounting solution. For the detection of osteoblasts, deplasticized and rehydrated sections were stained with 1% toluidine blue, pH 4.5, for one minute. For the detection of the osteoclasts, deplasticized and rehydrated sections were stained for the tartrate-resistant acid phosphatase activity. The sections were incubated with the substrate, 0.02% naphthol AS-BI phosphate solution, for 30 minutes under acidic conditions. Next, sodium nitrite (0.08% final concentration) and pararosaniline dye solution (0.08% final concentration) were added to the substrate solution containing the slides and left for ten minutes until the osteoclasts developed the characteristic red stain. Slides were counterstained with Carazzi's haematoxylin, washed in water and mounted using an aqueous medium. Stained bone sections were analyzed for bone volume/tissue volume (BV/TV), osteoid volume/bone volume (OV/BV), osteoblast and osteoclast count using the Osteomeasure software (Osteometrics Inc., Atlanta, Georgia). The region of interest was selected within the fracture healing site. Images were taken at room temperature using a light microscope (DM200; Leica, Wetzlar, Germany). All histological images were captured using a camera, acquired with DP2-BSW software (XV3.0; Olympus, Tokyo, Japan) and processed using Photoshop (Adobe, San Jose, California).

Three-point bending test. The stored bone samples were equilibrated at room temperature and placed on fulcra 5 mm apart. An axial load from above was applied on the fracture site between the two fulcra. The load was applied at a rate of 5 mm/minute until the bone breakage. This test was done using a universal three-point bending machine (Instron, Norwood, Massachusetts).

Statistical analysis. All statistical analyses were performed using SPSS software version 20 (IBM, Armonk, New York). Statistical analyses were performed by Student's *t*-test with $p < 0.05$ considered statistically significant. A single asterisk indicates $p < 0.05$, double asterisks indicate $p < 0.001$ and triple asterisks indicate $p < 0.0001$.

Results

Study design and surgery. Outlines of the study design and the surgical procedure have been depicted in Figure 1.

Radiographic analysis. The radiograph analyses provided the first line of evidence that PHOSPHO1 deficiency affected bone fracture healing. As shown in Figure 2a, WT fractured tibia showed a normal reduction of callus size four weeks after fracture, indicating that the formed callus had been remodelled and the tibia had returned to its uniform shape. On the other hand, the *Phospho1*$^{-/-}$ tibia showed the presence of a large callus indicative of delayed remodelling, suggesting that the fractured bone had not regained its original shape by the time of analysis.

μCT analyses. The cross-sectional μCT images of the WT and *Phospho1*$^{-/-}$ callus showed significant differences in both the shape and architecture of the bone at the fracture site (Fig. 2b). The WT tibia showed organized thick cortices with less trabecular bone in contrast to the *Phospho1*$^{-/-}$ callus that showed very thin cortices with an abundance of disorganized trabeculae.

The mean bone volume at the fracture site was found to be slightly higher in the WT (6.79 SD 0.58) than in the *Phospho1*$^{-/-}$ group (5.47 SD 0.71) although this was not significant (Student's *t*-test: $p = 0.175$) (Fig. 2c). Similarly, the percentage ratio of bone volume to tissue volume that was calculated for each group was found to be comparable in the WT (51.43 SD 0.177) and in the *Phospho1*$^{-/-}$ group (50.34 SD 2.9), without any significant differences (Student's *t*-test: $p = 0.757$) (Fig. 2d).

We also investigated other properties of the newly formed trabecular bone in the callus. The trabecular thickness and separation was significantly higher in the WT group (0.13 SD 0.003 and 0.22 SD 0.02) than in the *Phospho1*$^{-/-}$ group (0.09 SD 0.01 and 0.16 SD 0.02; $p = 0.008$ and $p = 0.03$, respectively) (Figs 2e and 2f). In contrast, the trabecular numbers were found to be significantly increased in the *Phospho1*$^{-/-}$ mice (5.70 SD 0.75) in comparison with WT mice (3.82 SD 0.18; $p = 0.03$) (Fig. 2g).

Histology and histomorphometric analyses. Histological analysis of the von Kossa-van Gieson-stained sections showed that the WT callus was more homogeneous with uniform cortices with minimal amounts of osteoid and trabecular bone (Fig. 3a). After visual comparison of the

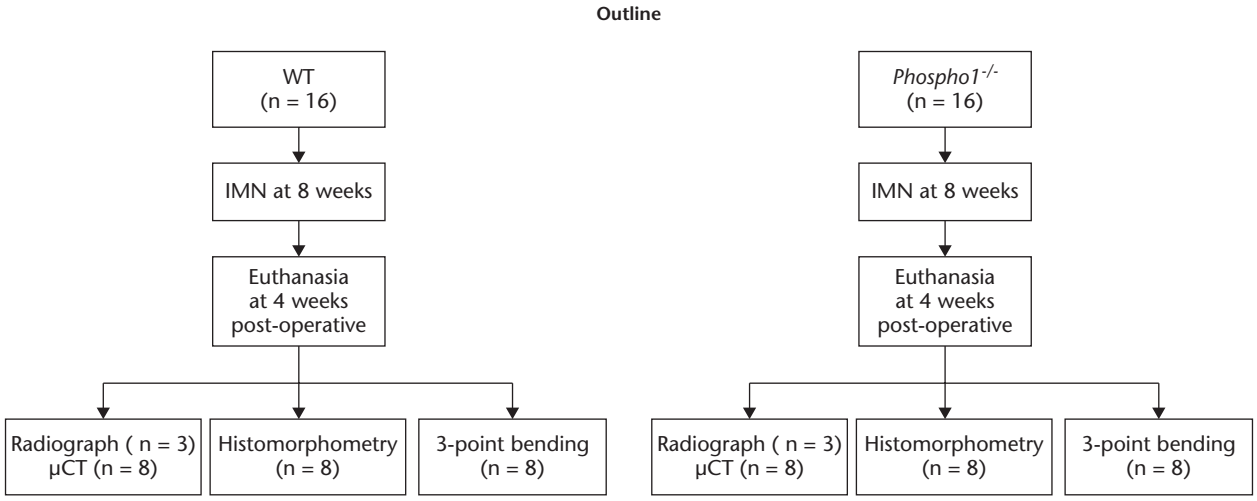

Fig. 1a

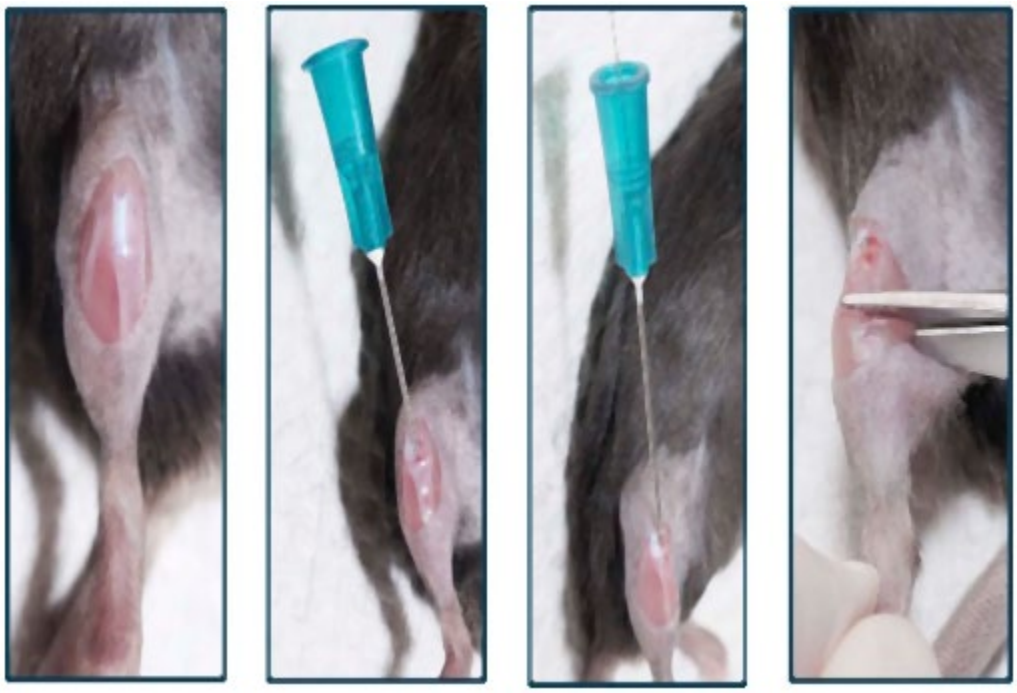

Fig. 1b

a) Scheme showing the study design. b) intramedullary nails (IMN) were inserted into the right tibia of eight-week-old (8w) wild-type (WT) and *Phospho1*$^{-/-}$ mice, which were then fractured. Mice were analyzed after four weeks (4w) of surgery by radiography, micro-CT (µCT), histomorphometry and three-point bending tests; steps of intramedullary fracture surgery of the tibia.

fractured bone sections in each group, there appeared to be an increase in the osteoid volume and surface area in the *Phospho1*$^{-/-}$ group. In addition, the callus appeared less organized and the cortices were poorly defined. At higher magnifications (Figs 3b and 3c), we observed an abundant amount of disorganized osteoid in the *Phospho1*$^{-/-}$ callus compared with the minimal amounts of evenly distributed osteoid in the WT callus.

To further confirm these observations, histomorphometric analyses were performed. The osteoid surface/bone surface (OS/BS) and OV/BV were measured in both groups. Both OS/BS and OV/BV in the *Phospho1*$^{-/-}$ group were significantly higher (34.82 SD 4.83 and 11.18 SD 0.68; $p = 0.007$) than in the WT group (7.74 SD 2.1 and 1.10 SD 0.12; $p = 0.0001$) (Fig. 4a).

The number of osteoblasts and osteoclasts per tissue area (N.Ob/T.Ar, N.Oc/T.Ar), and osteoblast and osteoclast surface per bone surface (Ob.s/BS, Oc.s/BS) were determined and the *Phospho1*$^{-/-}$ group showed a significant increase in osteoblast numbers in both the tissue (N.Ob/T.Ar) and on the bone surface (Ob.s/BS) when compared with the WT group ($p = 0.018$ and $p = 0.006$,

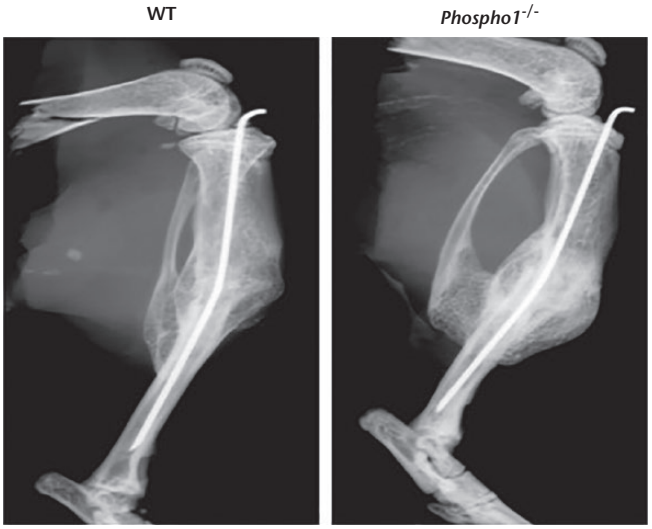

Fig. 2a

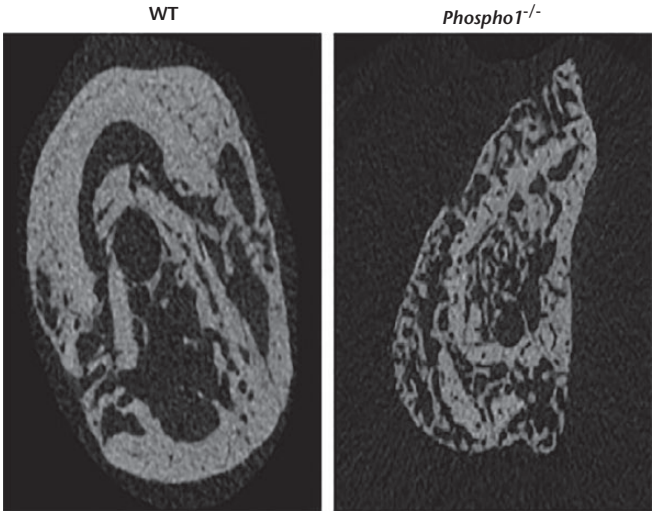

Fig. 2b

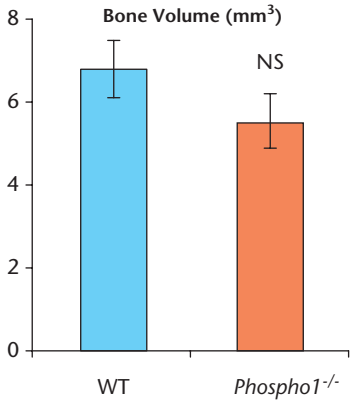

Fig. 2c

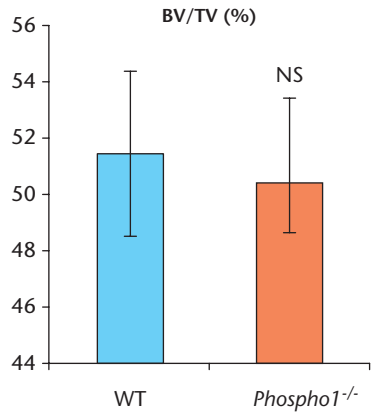

Fig. 2d

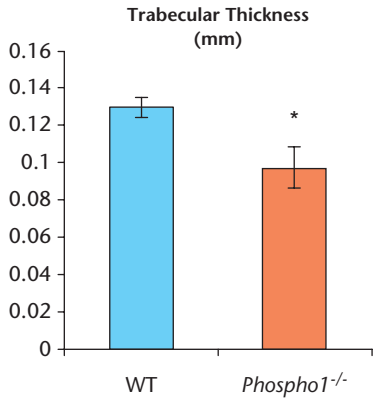

Fig. 2e

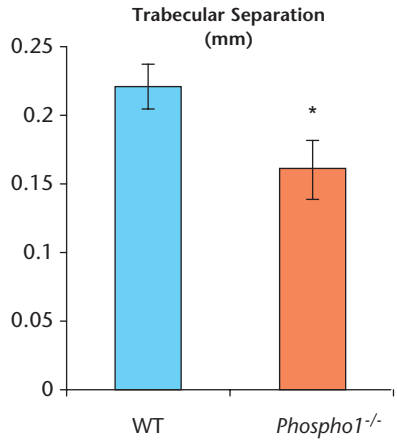

Fig. 2f

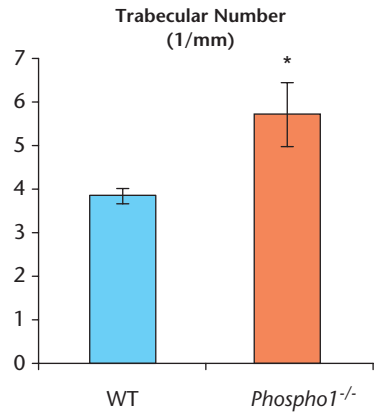

Fig. 2g

a) Radiographs of the fractured right tibia. There was an increase in callus size in *Phospho1*$^{-/-}$ fractured bone in comparison with wild-type (WT) bone; b) micro-CT (μCT) images of the site of fracture of the right tibia in WT and *Phospho1*$^{-/-}$ mice. WT fracture showed thick cortical walls with normal trabecular bone structure. *Phospho1*$^{-/-}$ fracture showed thin cortical walls and disorganized trabecular bones; c) and d) analysis of μCT data showed that there was no significant difference in total bone volume and bone volume/tissue volume (BV/TV) between WT and *Phospho1*$^{-/-}$ mice; e) and f) μCT analysis showed a significant decrease in the trabecular thickness and trabecular separation in *Phospho1*$^{-/-}$ fractured bone; g) trabecular numbers were significantly increased in *Phospho1*$^{-/-}$ fractured bones in comparison with WT fractured bones (NS, not significant).

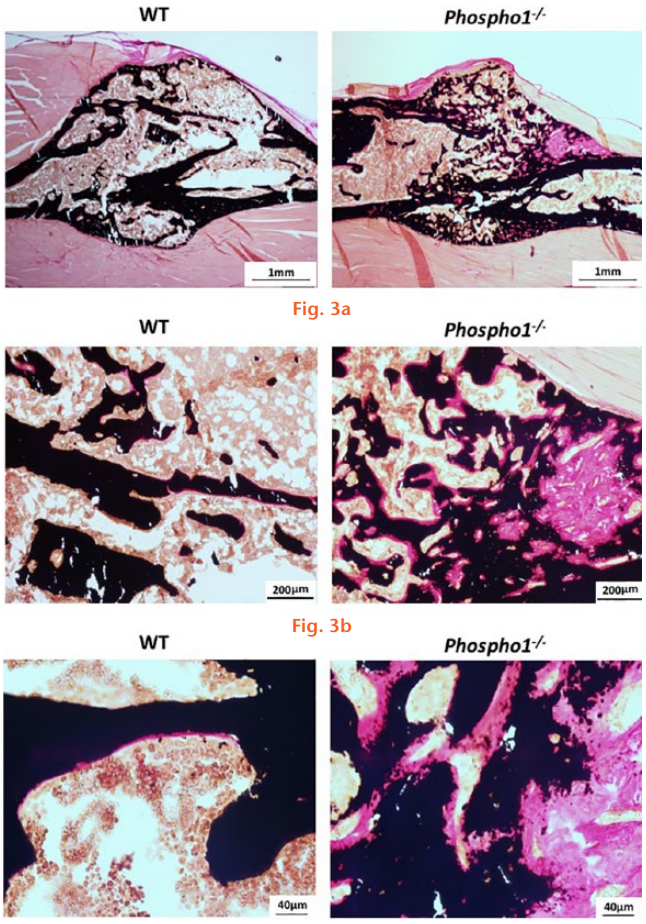

Microscopic images of tibia sections showing the fracture site. The sections were stained as per von Kossa and van Gieson, which stains unmineralized bone pink and mineralized bone black: a) wild-type (WT) sections showing normal fracture healing with a minimal amount of trabecular bone and evenly distributed osteoid. On the other hand, the *Phospho1*$^{-/-}$ fracture sections showed increased trabecular number and the osteoid formation. Panels (b) and (c) show the magnified view of the fractured bone sections.

respectively) (Fig. 4b) but osteoclast numbers were not significantly different between the two groups ($p = 0.25$ for both measurements) (Fig. 4c).

Mechanical analysis (three-point bending test). The mechanical properties of the fracture callus in the two groups was investigated. Three-point bending analysis showed that in the *Phospho1*$^{-/-}$ group, there was significantly more plastic deformation (load at yield) and a higher load to failure (maximum load) (Figs 5a and 5b) and this was statistically significant between the two groups ($p = 0.014$ and $p = 0.009$, respectively). In addition, the work required to reach this deformity and maximum load was significantly greater in the *Phospho1*$^{-/-}$ group ($p = 0.02$ and $p = 0.04$, respectively) (Figs 5c to 5e).

Discussion

Fracture union closely reflects the embryonic development of skeletal tissues, with a sequence of steps that require both systemic and local factors as well as coordinated functions of three cell types: chondrocytes and osteoblasts of mesenchymal origin, and osteoclasts from the hematopoietic lineage.[4,23] The activities of these cells are directly associated with ECM mineralization as both chondrocytes and osteoblasts are involved in the synthesis and mineralization of the organic matrix in the newly synthesized cartilage and bone, respectively, while osteoclasts resorb the mineralized ECMs in both of these tissues.[24,25] These cellular activities ultimately shape the architecture of the mineralized tissue at the fracture site and determine its biomechanical properties.

ECM mineralization, a specialized feature of skeletal tissues, is the basis of its unique physical and mechanical properties. Poor bone mineralization can result in skeletal deformities, which can in turn result in a variety of debilitating conditions.[26] Although poorly mineralized bone has been identified as a risk factor for pathological fractures, the effect of impaired mineralization on fracture healing has not been thoroughly studied.

While the effects of bone mineralization status on fracture healing is poorly understood, it has been shown that in elderly patients with bone fractures, vitamin D combined with dietary phosphate supplementation will promote the healing process.[27] Considering that the pro-mineralization effects of this treatment help fracture healing, we hypothesized that impaired cartilage and/or bone mineralization would have an adverse effect on fracture healing. To investigate this further, we have used a genetic model of osteomalacia that lacks PHOSPHO1, a phosphatase that functions predominantly in the mineralizing skeletal cells.

At present, the mode of action of PHOSPHO1 in the regulation of ECM mineralization is not well understood. The osteomalacia seen in *Phospho1*$^{-/-}$ mice is not caused by a systemic reduction of P_i or calcium levels, suggesting that PHOSPHO1 deficiency affects local cell-intrinsic factors that may be responsible for the observed phenotype.[28,29] It has been suggested that PHOSPHO1 activity is required for the initiation of hard tissue mineralization within the matrix vesicles (MVs), small membrane-enclosed bodies that are released by the mineralizing cells to provide a protected microenvironment for initial mineral crystal nucleation.[29] PHOSPHO1 activity within the MVs may increase the levels of P_i, triggering its precipitation as calcium phosphate salts. In support of this hypothesis, it has been shown that PHOSPHO1 is present and active in MV preparations,[16,29-32] and in addition, PHOSPHO1 is also required for the mineralization of the MVs.[15]

Reported literature and our unpublished data clearly show that PHOSPHO1 deficiency has an adverse effect on both cartilage and bone mineralization in endochondral ossification[15,21] and, therefore, we decided to use this mouse model to investigate fracture healing of the tibia with stabilization of the fracture with an intramedullary pin, a widely used technique to study fracture healing via endochondral ossification.

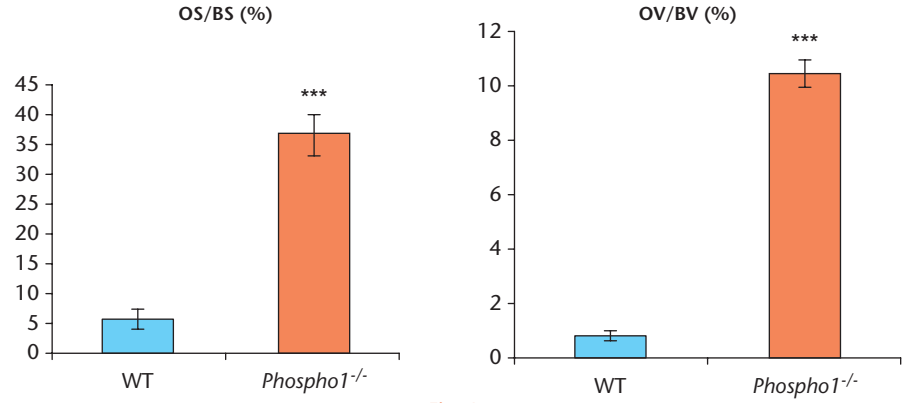

Fig. 4a

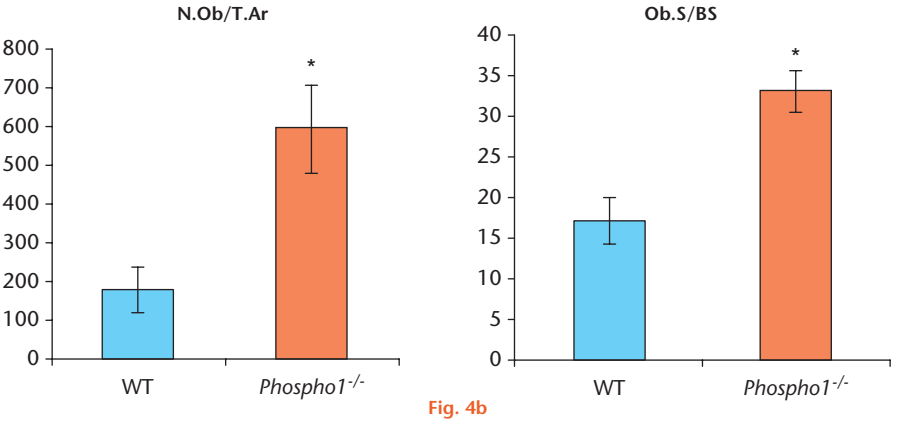

Fig. 4b

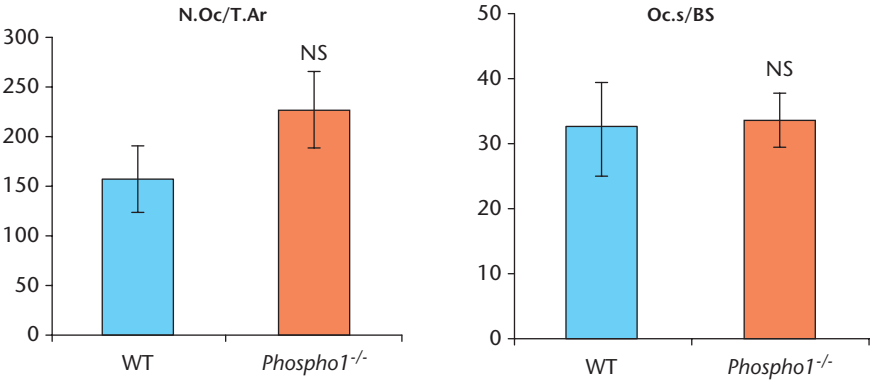

Fig. 4c

a) Histomorphometry on von Kossa and van Gieson-stained slides shows that there is a statistically significant increase in osteoid surface/bone surface (OS/BS) and osteoid volume/bone volume (OV/BV) in *Phospho1*$^{-/-}$ fractured bone sections; b) analysis of toluidine blue-stained sections showed a significant increase in the osteoblast count and surface area in *Phospho1*$^{-/-}$ fracture sites; c) analysis of tartrate-resistant acid phosphatase-stained sections showed that there was no statistically significant difference in the osteoclast count between the two groups (N.Ob, number of osteoblasts; T.Ar, tissue area; Ob.s, osteoblast surface; N.Oc, number of osteoclasts; Oc.s, osteoclast surface).

Although μCT analyses did not show a difference in bone volume at the fracture site between the two groups, with histomorphometric analysis, we were able to demonstrate a higher osteoid volume in the *Phospho1*$^{-/-}$ fracture sites. Apart from the cell-intrinsic mineralization defects, other possible explanations of this increase in osteoid volume at the fracture site of the mutant mice could be the combined effects of localized increase of bone formation by osteoblasts and the impaired osteoclast resorption of the unmineralized bone matrix. Indeed, this is supported by our observation that osteoblast numbers were higher in *Phospho1*$^{-/-}$ fracture sites, whilst osteoclast numbers were unchanged as compared with the WT fracture group. It has been reported that the unmineralized bone matrix does not remodel due to impaired resorption of the matrix by osteoclasts.[33-35] We believe that the increased synthesis of unmineralized bone and its poor resorption cause a significant delay in

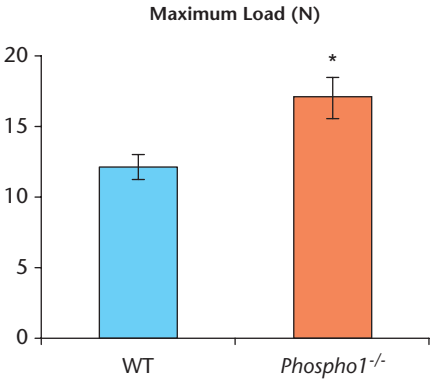

Fig. 5a

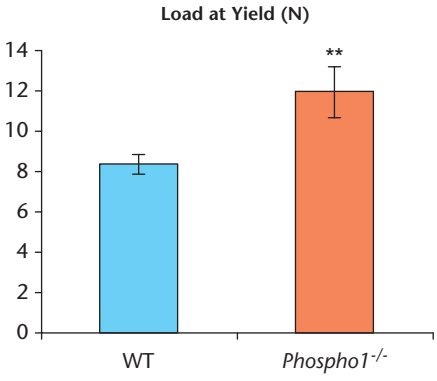

Fig. 5b

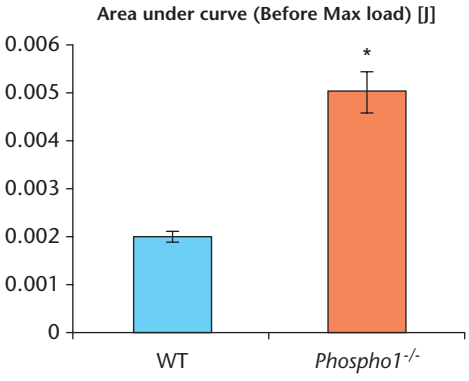

Fig. 5c

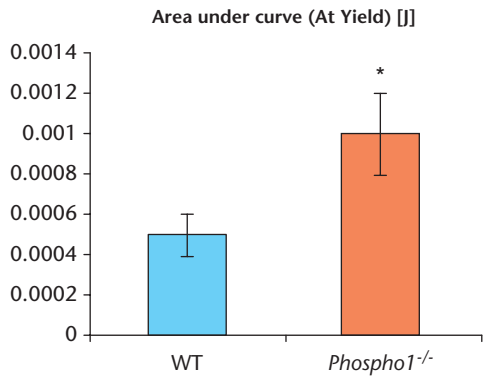

Fig. 5d

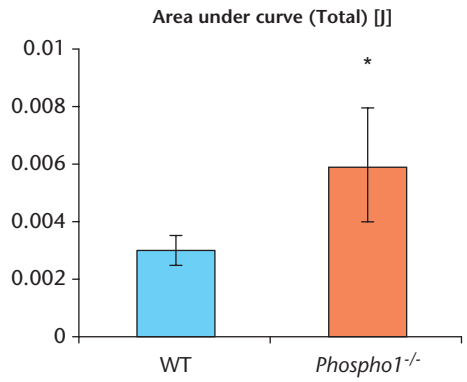

Fig. 5e

a) *Phospho1*$^{-/-}$ fractured bones required more load in order to break than the wild-type (WT) fractured bones; b) a significantly higher load was needed to cause a plastic deformity in the *Phospho1*$^{-/-}$ bone (load at yield) than in the WT bone; c) to e) overall, *Phospho1*$^{-/-}$ fractured bones needed more energy to deform and break in comparison with WT fractured bones as the former can sustain higher elastic and plastic deformities.

bone remodelling in the *Phospho1*$^{-/-}$ callus, resulting in inadequate fracture healing and weaker bone.

Three-point bending tests allowed us to investigate the mechanical properties of the fractured tibia. In normally mineralized bone, the load at yield (load required to produce permanent deformation of the bone) will be close to the maximal load (load to bone failure) and this will result in limited plastic deformation of the bone. In contrast, in poorly mineralized bone, there is a larger difference between these two mechanical properties and this will result in greater plastic deformation before fracture.[36,37] Callus will have different biomechanical properties at various stages of the fracture healing process. In the early stages of callus development, it will have limited strength but as the callus progressively matures, the strength and stiffness increases.[38,39]

In this study, we analyzed the bones at four weeks after fracture surgery, which is the normal length of time required for the fracture to heal in mice.[40] After four weeks, healed bone would be expected to be biomechanically competent. Our analysis showed that *Phospho1*$^{-/-}$ healed bones would tolerate greater loads before plastic deformation or ultimate failure in comparison with the WT healed bones. This increased elasticity of the newly formed PHOSPHO1-deficient callus can be explained by the increased amount of unmineralized bone compared with the mineralized bones found in the WT callus. In addition, this finding is consistent with the greenstick fracture in *Phospho1*$^{-/-}$ mice and pathological fractures that have been reported.[15]

In conclusion, our study has shown that PHOSPHO1 produced by bone-forming osteoblasts plays a key role in the normal bone fracture healing and in the formation of mechanically competent callus. We believe that this study has contributed to the existing body of knowledge about the role of PHOSPHO1 in bone mineralization and fracture healing. Further studies are needed to determine the clinical implications of these findings and whether PHOSPHO1 can be used as a therapeutic agent in the treatment of poorly mineralized fractured bone.

References

1. **Frost HM.** The biology of fracture healing. An overview for clinicians. Part I. *Clin Orthop Relat Res* 1989;248:283-293.
2. **Claes L, Recknagel S, Ignatius A.** Fracture healing under healthy and inflammatory conditions. *Nat Rev Rheumatol* 2012;8:133-143.
3. **Frost HM.** Skeletal physiology and bone remodeling. In: Urist MR, ed. *Fundamental and Clinical Bone Physiology*. Philadelphia: Lippincott, 1980:208-241.
4. **Einhorn TA.** The cell and molecular biology of fracture healing. *Clin Orthop Relat Res* 1998;355S(Suppl):S7-S21.
5. **Marks SC Jr, Popoff SN.** Bone cell biology: the regulation of development, structure, and function in the skeleton. *Am J Anat* 1988;183:1-44.

6. **Boskey AL, Robey PG.** The Composition of Bone. In: Bouillon R, Compston JE, eds. *Primer on the Metabolic Bone Diseases and Disorders of Mineral Metabolism*. Eighth ed. Wiley-Blackwell, 2013:32-38.
7. **Young MF.** Bone matrix proteins: their function, regulation, and relationship to osteoporosis. *Osteoporos Int* 2003;14(Suppl 3):S35-S42.
8. **Murshed M.** Mechanism of bone mineralization. *Cold Spring Harb Perspect Med* 2018 April 02. (Epub ahead of print)
9. **Millán JL.** The role of phosphatases in the initiation of skeletal mineralization. *Calcif Tissue Int* 2013;93:299-306.
10. **Hessle L, Johnson KA, Anderson HC, et al.** Tissue-nonspecific alkaline phosphatase and plasma cell membrane glycoprotein-1 are central antagonistic regulators of bone mineralization. *Proc Natl Acad Sci USA* 2002;99:9445-9449.
11. **Moss DW, Eaton RH, Smith JK, Whitby LG.** Association of inorganic-pyrophosphatase activity with human alkaline-phosphatase preparations. *Biochem J* 1967;102:53-57.
12. **Majeska RJ, Wuthier RE.** Studies on matrix vesicles isolated from chick epiphyseal cartilage. Association of pyrophosphatase and ATPase activities with alkaline phosphatase. *Biochim Biophys Acta* 1975;391:51-60.
13. **Fedde KN, Blair L, Silverstein J, et al.** Alkaline phosphatase knock-out mice recapitulate the metabolic and skeletal defects of infantile hypophosphatasia. *J Bone Miner Res* 1999;14:2015-2026.
14. **Narisawa S, Fröhlander N, Millán JL.** Inactivation of two mouse alkaline phosphatase genes and establishment of a model of infantile hypophosphatasia. *Dev Dyn* 1997;208:432-446.
15. **Yadav MC, Simao AM, Narisawa S, et al.** Loss of skeletal mineralization by the simultaneous ablation of PHOSPHO1 and alkaline phosphatase function: a unified model of the mechanisms of initiation of skeletal calcification. *J Bone Miner Res* 2011;26:286-297.
16. **Roberts SJ, Stewart AJ, Sadler PJ, Farquharson C.** Human PHOSPHO1 exhibits high specific phosphoethanolamine and phosphocholine phosphatase activities. *Biochem J* 2004;382:59-65.
17. **Roberts SJ, Stewart AJ, Schmid R, et al.** Probing the substrate specificities of human PHOSPHO1 and PHOSPHO2. *Biochim Biophys Acta* 2005;1752:73-82.
18. **Stewart AJ, Schmid R, Blindauer CA, Paisey SJ, Farquharson C.** Comparative modelling of human PHOSPHO1 reveals a new group of phosphatases within the haloacid dehalogenase superfamily. *Protein Eng* 2003;16:889-895.
19. **Houston B, Paton IR, Burt DW, Farquharson C.** Chromosomal localization of the chicken and mammalian orthologues of the orphan phosphatase PHOSPHO1 gene. *Anim Genet* 2002;33:451-454.
20. **Nielsen H, Engelbrecht J, Brunak S, von Heijne G.** Identification of prokaryotic and eukaryotic signal peptides and prediction of their cleavage sites. *Protein Eng* 1997;10:1-6.
21. **Macrae VE, Davey MG, McTeir L, et al.** Inhibition of PHOSPHO1 activity results in impaired skeletal mineralization during limb development of the chick. *Bone* 2010;46:1146-1155.
22. **Huesa C, Yadav MC, Finnilä MA, et al.** PHOSPHO1 is essential for mechanically competent mineralization and the avoidance of spontaneous fractures. *Bone* 2011;48:1066-1074.
23. **Bruder SP, Fink DJ, Caplan AI.** Mesenchymal stem cells in bone development, bone repair, and skeletal regeneration therapy. *J Cell Biochem* 1994;56:283-294.
24. **Teitelbaum SL.** Bone resorption by osteoclasts. *Science* 2000;289:1504-1508.
25. **Shapiro F.** Bone development and its relation to fracture repair. The role of mesenchymal osteoblasts and surface osteoblasts. *Eur Cell Mater* 2008;15:53-76.
26. **Khavandgar Z, Poirier C, Clarke CJ, et al.** A cell-autonomous requirement for neutral sphingomyelinase 2 in bone mineralization. *J Cell Biol* 2011;194:277-289.
27. **Schalin-Jäntti C, Mornet E, Lamminen A, Välimäki MJ.** Parathyroid hormone treatment improves pain and fracture healing in adult hypophosphatasia. *J Clin Endocrinol Metab* 2010;95:5174-5179.
28. **Stewart AJ, Roberts SJ, Seawright E, et al.** The presence of PHOSPHO1 in matrix vesicles and its developmental expression prior to skeletal mineralization. *Bone* 2006;39:1000-1007.
29. **Roberts S, Narisawa S, Harmey D, Millán JL, Farquharson C.** Functional involvement of PHOSPHO1 in matrix vesicle-mediated skeletal mineralization. *J Bone Miner Res* 2007;22:617-627.
30. **Golub EE.** Role of matrix vesicles in biomineralization. *Biochim Biophys Acta* 2009;1790:1592-1598.
31. **Anderson HC, Garimella R, Tague SE.** The role of matrix vesicles in growth plate development and biomineralization. *Front Biosci* 2005;10:822-837.
32. **Houston B, Stewart AJ, Farquharson C.** PHOSPHO1-A novel phosphatase specifically expressed at sites of mineralisation in bone and cartilage. *Bone* 2004;34:629-637.
33. **Bar-Shavit Z.** The osteoclast: a multinucleated, hematopoietic-origin, bone-resorbing osteoimmune cell. *J Cell Biochem* 2007;102:1130-1139.
34. **Vaes G.** Cellular biology and biochemical mechanism of bone resorption. A review of recent developments on the formation, activation, and mode of action of osteoclasts. *Clin Orthop Relat Res* 1988;231:239-271.
35. **Chambers TJ, Fuller K.** Bone cells predispose bone surfaces to resorption by exposure of mineral to osteoclastic contact. *J Cell Sci* 1985;76:155-165.
36. **Mazzocca A, Browner B, et al.** Principles of Internal Fixation. In: Browner B, Levine A, Jupiter J, Trafton P, Krettek C, eds. *Skeletal Trauma*. Philadelphia: Saunders, 2003:293-298.
37. **Turner CH, Burr DB.** Basic biomechanical measurements of bone: a tutorial. *Bone* 1993;14:595-608.
38. **White AA III, Panjabi MM, Southwick WO.** The four biomechanical stages of fracture repair. *J Bone Joint Surg [Am]* 1977;59-A:188-192.
39. **Morgan EFaTAE.** Biomechanics of fracture healing. In: Bouillon R, Compston JE, eds. *Primer on the Metabolic Bone Diseases and Disorders of Mineral Metabolism*. Eighth ed. Hoboken: Wiley-Blackwell, 2013:65-69.
40. **Mills LA, Simpson AH.** In vivo models of bone repair. *J Bone Joint Surg [Br]* 2012;94-B:865-874.

Funding Statement

- This work has been supported by a research grant (RGPIN-2017-06881) from the Natural Sciences and Engineering Research Council, Canada awarded to M. Murshed.

Author Contributions

- M. W. Morcos: Participated in experimental design, Performed experiments, Prepared the first draft and subsequent modification of the text.
- H. Al-Jallad: Performed experiments and contributed to manuscript preparation.
- J. Li: Performed experiments and contributed to manuscript preparation.
- C. Farquharson: Provided Phospho1-/- mice and contributed to manuscript preparation.
- J. L. Millán: Provided Phospho1-/- mice and contributed to manuscript preparation.
- R. C. Hamdy: Contributed to manuscript preparation.
- M. Murshed: Conceptualized and supervised the project, Contributed to manuscript preparation and approved the final version of the manuscript.

Conflict of Interest Statement

- None declared